Engineering Notes

Detumbling Attitude Control Analysis Considering an Electrostatic Pusher Configuration

Vladimir Aslanov*
Samara National Research University, Samara, 443086, Russian
and
Hanspeter Schaub†
University of Colorado, Boulder, Colorado 80309-0431

DOI: 10.2514/1.G003966

Nomenclature

a_p	=	acceleration of the space tug, m/s^2
C_1xy	=	local-vertical/local-horizontal coordinate
c_α	=	feedback control coefficient, m/s^2
c_v	=	feedback control coefficient, 1/s
c_ω	=	feedback control coefficient, m/s
$\boldsymbol{D}_i$	=	sum of the perturbation forces acting on the space tug and debris
$\boldsymbol{d}$	=	distance between the space tug and debris, m
$\boldsymbol{d}$	=	position vector of the debris relative to the space tug, m
$\boldsymbol{e}_x$	=	unit vector of the local vertical at the space tug position, m
$\boldsymbol{e}_y$	=	unit vector of the local horizontal at the space tug position, m
$\boldsymbol{F}_i$	=	net force acting on the space tug () and debris (), N
$\boldsymbol{F}_{1,2}$	=	Coulomb force acting on the debris, N
$\boldsymbol{F}_{2,1}$	=	Coulomb force acting on the space tug, N
$\boldsymbol{J}$	=	moment of inertia of the space debris, kg/m^2
k_c	=	Coulomb constant
m_i	=	mass of the space tug () and debris (), kg
m_1	=	mass of the tug, kg
m_2	=	mass of the debris, kg
n	=	mean motion of the space tug, rad/s
$\boldsymbol{P}$	=	tug's thrust force vector, N
q_i	=	craft charges and, C
$\boldsymbol{r}_i$	=	position vector of the space tug (i is equal to one) and debris (i is equal to two), m
U_x, U_y	=	projections of the control force, N
u_x, u_y	=	projections of the accelerations provided by the control forces U_x and U_y, m/s^2
α	=	angle between the local-horizontal line of the tug and the line connecting the tug and debris, rad
θ	=	pitch attitude angle
θ_s	=	equilibrium position

Received 22 July 2018; revision received 14 October 2018; accepted for publication 3 November 2018; published online 3 January 2019.

*Professor; aslanov_vs@mail.ru.
†Professor, Glenn L. Murphy Chair of Engineering, Department of Aerospace Engineering Sciences, 431 UCB, Colorado Center for Astrodynamics Research; hanspeter.schaub@colorado.edu.

I. Introduction

SPACE debris is a growing concern for both low-Earth-orbit (LEO) and geosynchronous orbit (GEO) regimes [1–3]. In particular, the comprehensive study in Ref. [2] discussed how zones within the GEO regime are becoming very congested, rivaling the worst LEO debris concerns. The defunct GEO satellites tend to be very large, often reaching beyond 5–10 m in size, as well as rotating and tumbling [4]. The act of docking onto such large and tumbling space objects is very challenging; as a result, novel touchless debris removal or despinning solutions are being explored. The ion-shepherd method uses the ion engine exhaust to push and/or despin a satellite [5], whereas the laser ablation method uses the debris' own mass as a thruster fuel source [6]. A promising touchless and low-power solution is the electrostatic tractor [7]. Here, active charge emission is used to both charge the tug or servicer vehicle as well as the debris object. Although the original concept uses an electron gun to charge the tug positive and debris negative, creating an attractive electrostatic tractor force, with auxiliary charge emission on the tug, it is also possible to charge both the servicer and debris to the same potential to create a repulsive force [8,9]. Most of the control research using the electrostatic tractor considers a pulling configuration to move GEO objects [10]. Earlier work considered the relative motion control for a pusher configuration but did not consider any attitude motion. Furthermore, modulated electrostatic tractor implementations were studied to detumble a space object without physical touch [11]. This enabled orbital servicing and docking missions to first remove a large amount of the rotational kinetic energy before physically docking and engaging with a satellite.

The aim of this Note is to investigate the control of the space tug and debris for the removal and detumbling of the space debris or defunct satellites using electrostatic forces. The goal is to provide a stable relative motion of the tug and the debris, both in terms of translation and rotation. With the spacecraft and debris nominally charged with the same polarity to consider a pusher configuration, a feedback control method using both the thrusters for station-keeping and the electrostatic charge modulation of the space tug for pushing and detumbling is considered. The feedback control laws align the tug–debris direction with the tug alongtrack orbit axis and maintain a nominally constant distance between the charged tug and debris, all while stabilizing the attitude motion of the debris. For the scope of this Note, only inplane motion of the tug and debris are considered. The tug is assumed as a sphere with a homogenous potential, and the debris is assumed as a rigid conducting cylindrical body that has nominal electric charges of the same sign; and the repulsive electrostatic forces act between the tug and the debris. Furthermore, the tug has two thrusters: the main thruster, which provides the acceleration of the whole system for the disposal of the debris to a disposal orbit; and the control thruster, which ensures the required position of the tug relative to the debris. This scenario covers general repositioning of both large and small GEO satellites, as well as moving large space debris to a disposal orbit that lies to 200–250 km above GEO.

II. Accurate Electrostatic Torque Approximations

A. Multisphere Model Overview

Modeling the electrostatic forces and torques between two three-dimensional conducting shapes is readily solved these days using numerical finite element programs. However, the time to evaluate a single solution can range from 1 min to tens of minutes, depending on the complexity of the scenario. To model the dynamics of two

neighboring charged space objects, these force evaluation times are orders of magnitude too large to be practical. Consider the GEO regime in which natural charging can reach tens of kilovolts with particular space weather conditions [12–16]. To numerically simulate the rotational motion of two charged GEOs for one orbit using a fourth-order Runge–Kutta integration method and a 0.1 s time step (common for attitude simulations), assuming a conservative 60 s per force evaluation using a finite element solver, would require 2400 days of computation time. Faster numerical methods are required to approximate the electrostatic forces and torques acting on a system of charged objects. The multisphere method (MSM) is a lower-fidelity electrostatic modeling technique that can be evaluated quickly enough for faster-than-realtime applications [17,18].

With the MSM the conducting spacecraft charge distribution is modeled through a series of spheres. The optimal locations of these spheres are found through either a force and torque [19] or an E-field matching technique [20]. Figure 1 illustrates a cylindrical rocket body being modeled through a set of three internal spheres. This MSM technique is called the volume MSM or VMSM. An alternate MSM technique, called the surface MSM or SMSM, populates the object's surface with a series of spheres [18]. The SMSM can yield more accurate approximations than the VMSM models, but the number of spheres makes any analytical formulations impractical. Assuming a two- to three-craft radii separation, either method can yield accuracies that are better than 1–2%.

The MSM is an elastance-based method for predicting the force and torque on conductors [21]. With either the VMSM or the SMSM technique, the mathematical formulation of the E forces and torques is the same. Assume the objects are represented through N_T conducting spheres for which the optimal body-fixed locations and sizes have been determined a priori. The $N_T \times 1$ charge matrix $\boldsymbol{q} = [\,q_1 \quad q_2 \quad \cdots \quad q_{N_T}\,]$, which contains the charge on each sphere of a MSM model, is related to the $N_T \times 1$ sphere voltage matrix $\boldsymbol{\Phi} = [\,\Phi_1 \quad \Phi_2 \quad \cdots \quad \Phi_{N_T}\,]$ through [17] the following:

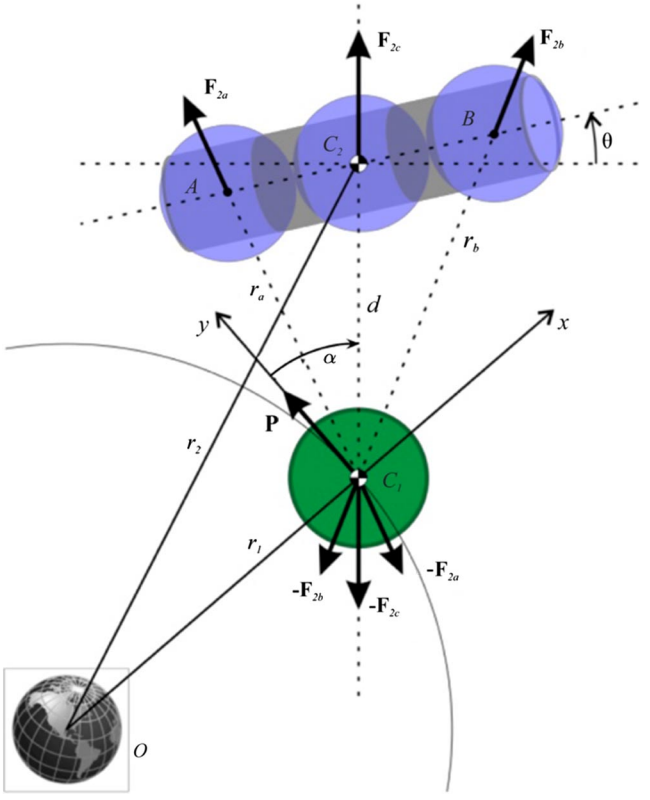

Fig. 1 Multisphere illustration of a tumbling cylinder neighboring a spherical tug.

$$\boldsymbol{q} = \frac{1}{k_c} C_M \boldsymbol{\Phi} \tag{1}$$

where $k_c = 1/(4\pi\epsilon_0)$ is the Coulomb constant, and the $N_T \times N_T$ matrix $(1/k_c)C_M$ is the position-dependent capacitance matrix. The inverse of C_M is the elastance matrix S, which is readily formulated as

$$S = k_c \begin{bmatrix} \frac{1}{R_1} & \frac{1}{r_{1,2}} & \cdots & \frac{1}{r_{1,N_T}} \\ \frac{1}{r_{1,2}} & \frac{1}{R_2} & \cdots & \frac{1}{r_{2,N_T}} \\ \vdots & \vdots & \ddots & \vdots \\ \frac{1}{r_{1,N_T}} & \frac{1}{r_{2,N_T}} & \cdots & \frac{1}{R_{N_T}} \end{bmatrix} \tag{2}$$

where R_i are the individual MSM sphere radii, and $r_{i,j}$ is the relative distance between spheres i and j. By knowing the potential Φ_i on each sphere, Eqs. (1) and (2) allow for the MSM charges q_i to be computed. The computational speed, or analytical complexity of the charge formulation, is directly dependent on how many MSM spheres are used. The VMSM approach yields good approximations with a small number of spheres for very rapid numerical force evaluations, as well as some analytical insight if only two to three spheres are used. The SMSM model provides enhanced fidelity because it can better model nonhomogenous charge distributions if the objects are very close to each other. However, instead of using two to three VMSM spheres, the SMSM approach uses tens or hundreds of spheres. Because the elastance matrix inverse is an N^3-order evaluation, the SMSM modeling is orders of magnitude slower than the VMSM solution but provides noticeable accuracy improvements if the craft are separated less than two to three craft radii.

To evaluate the general forces and torques, the Coulomb interactions are summed up across all the MSM spheres through

$$\boldsymbol{F} = -k_c \sum_{k=1}^{M} q_k \sum_{i=1}^{N} \frac{q_i}{\|r_{i,k}\|^3} \boldsymbol{r}_{i,k} \tag{3}$$

$$\boldsymbol{\tau} = -k_c \sum_{k=1}^{M} q_k \sum_{i=1}^{N} \frac{q_i}{\|r_{i,k}\|^3} \boldsymbol{r}_{C_2,i} \times \boldsymbol{r}_{i,k} \tag{4}$$

Here, the Debye shield of the local plasma environment is ignored because the separation distance considered of 10–25 m is significantly less than the average minimum GEO Debye length of 200 m.

Next, the specific scenario is considered where the MSM modeling is used for a debris–tug dynamical system, as illustrated in Fig. 1. Here, the tug is modeled through a single sphere C_1 and the cylindrical debris is modeled through three spheres: A, B, and C_2. The conducting debris object has the potential Φ_D, and the conducting spherical tug has the potential Φ_T. The charge–voltage relationship is now partitioned as

$$\begin{bmatrix} \Phi_D \\ \Phi_D \\ \Phi_D \\ \Phi_T \end{bmatrix} = k_c \begin{bmatrix} & & & \vdots & \\ & S_D & & \vdots & S_{D,T} \\ & & & \vdots & \\ \cdots & \cdots & \cdots & \cdots & \cdots \\ & S_{D,T}^T & & \vdots & S_R \end{bmatrix} \begin{bmatrix} q_a \\ q_b \\ q_{c_2} \\ \cdots \\ q_{c_1} \end{bmatrix} \tag{5}$$

where the elastance matrix partitions are defined as

$$S_D = \begin{bmatrix} \frac{1}{R_a} & \frac{1}{r_{a,b}} & \frac{1}{r_{a,c_2}} \\ \frac{1}{r_{a,b}} & \frac{1}{R_a} & \frac{1}{r_{b,c_2}} \\ \frac{1}{r_{a,c_2}} & \frac{1}{r_{b,c_2}} & \frac{1}{R_{c_2}} \end{bmatrix} \tag{6a}$$

$$S_{D,T} = \begin{bmatrix} \frac{1}{r_{a,c_1}} & \frac{1}{r_{b,c_1}} & \frac{1}{r_{c_2,c_1}} \end{bmatrix}^T \tag{6b}$$

$$S_T = \begin{bmatrix} \frac{1}{R_{c_1}} \end{bmatrix} \tag{6c}$$

Note that the inverses of S_D and S_T yield the self-capacitance matrix of the debris and tug, respectively; whereas the mutual capacitance between them is the $S_{D,T}$ partition. Using the Schur complement matrix decomposition [22] to express the elastance matrix inverse allows Eq. (5) to be solved for the charges using the following:

$$\begin{bmatrix} q_a \\ q_b \\ q_{c_2} \end{bmatrix} = \frac{1}{k_c}(\Gamma \boldsymbol{\Phi}_D - \Gamma S_{D,T} S_T^{-1} \Phi_T) \tag{7a}$$

$$q_{c_1} = \frac{1}{k_c}(-S_T^{-1} S_{D,C}^T \Gamma \boldsymbol{\Phi}_D + (S_T^{-1} + S_T^{-1} S_{D,C}^T \Gamma S_{D,T} S_T^{-1})\Phi_T) \tag{7b}$$

where

$$\Gamma = (S_D - S_{D,T} S_T^{-1} S_{D,T}^T) \tag{8}$$

and

$$\boldsymbol{\Phi}_D = [\,\Phi_D \quad \Phi_D \quad \Phi_D\,]^T \tag{9}$$

The mutual elastance component $S_{D,T}$ accounts for the fact that two neighboring charged objects will influence each other's charge–voltage relationship. However, if the separation distance grows sufficiently large, this influence becomes negligible. If the MSM is used for a feedback control development, then the charge evaluations in Eq. (7) are rendered much more complex if this mutual capacitance term is included. If $S_{D,T}$ can be assumed to be small, then the charge equations in Eq. (7) simplify to the two isolated body solutions:

$$\begin{bmatrix} q_a \\ q_b \\ q_{c_2} \end{bmatrix} = \frac{1}{k_c} S_D^{-1} \boldsymbol{\Phi}_D \tag{10a}$$

$$q_{c_1} = \frac{1}{k_c} S_T^{-1} \Phi_T \tag{10b}$$

For the particular cylinder (debris) and sphere (tug) scenario illustrated in Fig. 1, the total electrostatic force onto the cylinder is then given by [17,19]

$$\boldsymbol{F}_{E2} = -\boldsymbol{F}_{E1} = k_c |q_1| \sum_{i=a}^{c} \frac{q_i}{r_i 3} \boldsymbol{r}_i \tag{11}$$

whereas the force on each of the cylinder MSM spheres is given by

$$\boldsymbol{F}_{2,i} = k_c \frac{|q_1| q_i}{r_i 3} \boldsymbol{r}_i, \qquad i = a, b, c \tag{12}$$

The local-vertical/local-horizontal (LVLH) coordinate frame is used to describe the relative motion of two spacecraft. The origin of the LVLH frame is the center of mass of the space tug C_1. Axis $C_1 x$ is aligned with the local-vertical line, and the $C_1 y$ axis is aligned with the local-horizontal line (Fig. 1). We assume that the distance $r_b(t) = d(t)$ between the bodies is varied according to the motion equations of the debris and the tug.

B. Planar Rotational Equations of Motion

1. Attitude Motion

To describe the motion of the debris relative to its own mass center C_2, we use the angular momentum theorem:

$$\frac{\mathrm{d}}{\mathrm{d}t}[J(\dot{\theta} - \dot{\alpha} + \dot{f})] = L_E + L_G \tag{13}$$

where f is the true anomaly angle of the tug. Here, the electrostatic torque is

$$L_E = \frac{\partial \boldsymbol{r}_{ca}}{\partial \theta} \cdot \boldsymbol{F}_{2a} + \frac{\partial \boldsymbol{r}_{cb}}{\partial \theta} \cdot \boldsymbol{F}_{2b}, \qquad (\boldsymbol{r}_{ca} = \overline{CA}, \boldsymbol{r}_{cb} = \overline{CB}) \tag{14}$$

and the gravitational torque is

$$L_G = \frac{3n^2}{(1-e^2)^3}(1 + e\cos f)^3 (J - J_0) \sin(\theta - \alpha)\cos(\theta - \alpha) \tag{15}$$

where $J_x = J_y = J_0$ and $J = J_z$ are the moments of inertia of the cylindrical debris object.

The electrostatic torque in Eq. (14) is nontrivial due to the complexity of the determining Coulomb forces in Eq. (11) using the capacitance relation in Eqs. (5) and (6); to obtain analytical solutions, the symbolic manipulator Mathematica [23] is used. After some additional transformations, the electrostatic force is written as

$$\boldsymbol{F}_{E1} = (F_{E1,x}, F_{E1,y}) = -\frac{1}{H}(a_{E,x}[b_{E,x}\cos(\alpha - \theta) + c_{E,x}\sin\alpha], a_{E,y}[b_{E,x}\sin(\alpha - \theta) + a_{E,x}\cos\alpha]) \tag{16}$$

Here,

$$\begin{aligned} H(\theta, d) = {} & [-4d^2 l R_1 G_+^2 R_2 (l^2 - R_2 R_{2,c}) + 4dl R_1 G_- G_+ R_2 (2l G_+ R_{2,c} \\ & + R_2(dl - (2d + G_+)R_{2,c})) + G_-^2 (4dl R_1 G_+ (2l - R_2) R_2 R_{2,c} \\ & - 4d^2 l R_1 R_2 (l^2 - R_2 R_{2,c}) + G_+^2 (2l - R_2)(2l^2 (d^2 - R_1 R_{2,c}) \\ & + R_2 (d^2 l - (4d^2 + l R_1) R_{2,c})))]^2 \end{aligned} \tag{17}$$

$$G_\pm(\theta, d) = (l^2 \pm 2ld\sin\theta + d^2)^{1/2} \tag{18}$$

where $d = |\boldsymbol{r}_2 - \boldsymbol{r}_1| = \sqrt{x^2 + y^2}$ is the separation distance vector between the objects, θ is the cylinder orientation angle (Fig. 1), Φ_1 is the controlled voltages of the tug, and Φ is the constant voltages of the debris.

In Eq. (16), an unimportant assumption is used where $R_{2,b} = R_{2,a} = R_2$ and R_2 is the radius of cylinder 2 (debris).

2. Motion of the System Relative to the Inertial Frame

At first, the motion of the space tug and debris is considered in the Earth-centered inertial frame $OXYZ$. The origin of the $OXYZ$ frame is in the center of the Earth. The OXY plane coincides with the Earth's equatorial plane, the OX axis is aligned with the equinox, and the OZ axis extends through the North Pole. The positions of the space tug and space debris are described by the column vectors $\boldsymbol{r}_1 = [x_1, y_1]^T$ and $\boldsymbol{r}_2 = [x_2, y_2]^T$, respectively. The inertial equations of motion of the space tug and debris relative to the $OXYZ$ frame are as follows:

$$m_i \frac{\mathrm{d}^2 \boldsymbol{r}_i}{\mathrm{d}t^2} = -\mu \frac{\boldsymbol{r}_i}{r_i^3} + \boldsymbol{F}_i, \qquad i = 1, 2 \tag{19}$$

where the time derivatives are inertial derivatives of the vectors, m_i ($i = 1, 2$) are masses of the tug ($i = 1$) and debris ($i = 2$) objects, and $\boldsymbol{F}_i$ ($i = 1, 2$) are the net forces acting on the space tug ($i = 1$) and debris ($i = 2$):

$$\boldsymbol{F}_1 = U_x\boldsymbol{e}_x + (P + U_y)\boldsymbol{e}_y + \boldsymbol{F}_{E1} + \boldsymbol{N}_1 \tag{20}$$

$$\boldsymbol{F}_2 = \boldsymbol{F}_{E2} + \boldsymbol{N}_2 \tag{21}$$

where $\boldsymbol{N}_i$ is the net vector of other disturbance forces acting on the tug ($i = 1$) and the debris ($i = 2$), which include gravity perturbations of the sun and the moon, the solar pressure, and perturbations due to a nonspherical Earth's gravity. $P = \text{const}$ is the nominally constant station-keeping thrust force of the space tug. This thrust $\boldsymbol{P}$ is assumed to be aligned with the local-horizontal axis of the space tug.

The Coulomb forces acting between the objects are defined by Eq. (11):

$$\boldsymbol{F}_{E1} = -\boldsymbol{F}_{E2} = -(\boldsymbol{F}_{2a} + \boldsymbol{F}_{2b} + \boldsymbol{F}_{2c}) \tag{22}$$

These equations are nontrivial due to the complexity of the determining Coulomb forces in Eq. (11) through the elastance and capacitance matrices in Eqs. (5) and (6). To obtain analytical force solutions, the symbolic manipulator Mathematica [23] is used. Using Eq. (14), and after performing some additional transformations, the Coulomb force in Eq. (22) is written as

$$\boldsymbol{F}_{E1} = (F_{E1,x}, F_{E1,y}) = -\frac{1}{H}(a_{E,x}[b_{E,x}\cos(\alpha-\theta) + c_{E,x}\sin\alpha], a_{E,y}[b_{E,y}\sin(\alpha-\theta) + c_{E,y}\cos\alpha]) \tag{23}$$

where the $a_{E,x}, b_{E,x}, c_{E,x}, a_{E,y}, b_{E,y}$, and $c_{E,y}$ definitions are defined in the Appendix and allow for the compact expression in Eq. (23). Furthermore, the variable $\alpha = \arctan(-x/y)$ is the angle between the local-horizontal line of the tug and the line connecting the tug and debris.

The control thrusters of the space tug can produce thrust along the local-horizontal and local-vertical axes:

$$\boldsymbol{U} = U_x\boldsymbol{e}_x + U_y\boldsymbol{e}_y \tag{24}$$

The feedback control law of the space tug motion is developed using Eq. (19). However, because it is necessary to maintain a predetermined relative motion of two bodies during the active debris removal, maintaining a balance between the force $\boldsymbol{P}$ and the Coulomb interaction force, there is a good reason to use the equations of the relative motion. This is the subject of the next subsection. Equation (19) is used to validate the obtained feedback control law.

3. *Motion of the System in Euler–Hill Frame*

Let us consider the motion of the debris relative to the local-vertical/local-horizontal or Euler–Hill frame C_1xy [24] (Fig. 1) with the chief (tug) in a circular orbit. This is a good assumption for GEO debris object tugging. The rectilinear LVLH frame is attached to the space tug. The position of the debris relative to the space tug is described by the column vector

$$\boldsymbol{d} = \begin{bmatrix} x \\ y \end{bmatrix} \tag{25}$$

The LVLH frame is a noninertial frame, and so the equations of the debris relative to the space tug contain the terms associated with the motion of the LVLH frame relative to the Earth. The equation has the classical form [25]

$$\begin{aligned} \ddot{x} - 2n\dot{y} - 3n^2x &= a_x \\ \ddot{y} + 2n\dot{x} &= a_y \end{aligned} \tag{26}$$

where n is the orbital rate of the space tug, which is changed under the action of the tug's thrust. The change of the orbital rate $\dot{n}$ is approximated as

$$\dot{n} = \frac{P}{m_1 + m_2}\frac{1}{r} \tag{27}$$

where r is the distance from the Earth center to the center of mass of the system. The rate of change of n is close to zero due to the small value of the thrust force P, and so the value of $\dot{n}$ is neglected [25]. For example, electric thrusters have thrust output in the micro- to milli-Newton range. For $P = 20$ mN and $m_1 + m_2 = 5000$ kg,

$$\dot{n} = \frac{20\text{ mN}}{5000\text{ kg}} \cdot \frac{1}{35,786\text{ km}} \approx 10^{-13}\text{ s}^{-2} \tag{28}$$

This value is several orders of magnitude smaller than the magnitude of $n^2 \approx 5 \cdot 10^{-9}1/\text{s}^2$ presented in Eq. (26).

The right side of Eq. (26) includes projections of the acceleration produced by the main thruster and the control thrusters of the tug and by the electrostatic force:

$$\boldsymbol{a} = \begin{bmatrix} a_x \\ a_y \end{bmatrix} = -\boldsymbol{F}_{E1}\left(\frac{m_1 + m_2}{m_1 m_2}\right) - (\boldsymbol{a}_P + \boldsymbol{u}_x + \boldsymbol{u}_y) \tag{29}$$

where $\boldsymbol{a}_P$ is the acceleration of the space tug provided by the main engine thrust $\boldsymbol{P}$:

$$\boldsymbol{a}_p = \frac{P}{m_1}\begin{bmatrix} 0 \\ 1 \end{bmatrix} = \begin{bmatrix} 0 \\ a_p \end{bmatrix} \tag{30}$$

Note that $\boldsymbol{u}_x$ and $\boldsymbol{u}_y$ are the accelerations created by the control engines' thrust U_x and U_y:

$$u_x = U_x/m_1, \qquad u_y = U_y/m_1 \tag{31}$$

Next, the relative equations of motion are rewritten using polar coordinates α and d that are more suitable to use during the analysis of relative motion. Substituting $x = d\sin\alpha$, $y = d\cos\alpha$, and their derivatives into the relative equations of motion leads to

$$\ddot{\alpha} = 2\frac{n - \dot{\alpha}}{d}\dot{d} + \frac{3}{2}n^2\sin 2\alpha + \frac{1}{d}[(a_p + u_y)\sin\alpha - u_x\cos\alpha] + \frac{1}{m_* d}(F_{E1,x}\cos\alpha - F_{E1,y}\sin\alpha) \tag{32}$$

$$\ddot{d} = d(3n^2\sin^2\alpha - 2n\dot{\alpha} + \dot{\alpha}^2) - (u_y + a_p)\cos\alpha - u_x\sin\alpha - \frac{1}{m_*}(F_{E1,x}\sin\alpha + F_{E1,y}\cos\alpha) \tag{33}$$

where $m_* = m_1 m_2/(m_1 + m_2)$ is the reduced mass of the system.

III. Simplified Nonlinear Model

Reference [26] shows how to steer a tug for sustainable motion of the system, considering the debris as a simple point-charge model. However, this did not consider any attitude motion and electrostatic torques. Now, considering the debris as a solid body, an electrostatic tug charge feedback control algorithm is found to stabilize the debris attitude motion relative to the line connecting mass centers between the tug and the debris. The very complicated forms of the formulas for the electrostatic torque in Eq. (16) and the forces in Eq. (23) make this a challenging task. The following assumptions are used to simplify these formulas, and hence the equations of motion described in Eqs. (13), (32), and (33). So, assume that the length l of the cylinder body 2 (Fig. 1) is much less than the distance d between the centers of mass of two bodies:

$$\lambda = \frac{l}{d} \ll 1 \tag{34}$$

With this assumption, the induced charge effects are considered negligible, which lead to a significant reduction in the electrostatic

torque and force evaluation. Thus, the Coulomb torque in Eq. (16) and the forces in Eq. (23) are simplified to the following expressions:

$$L_E(\theta, d) = \lambda^3 \frac{3R_1}{2k_c d^2}\Phi_1\left(\frac{R_1}{3d}\Phi_1 + \Phi_2\right)\sin 2\theta \tag{35}$$

$$\boldsymbol{F}_{E1} = (F_{E1,x}, F_{E1,y}) = -\lambda\frac{7R_1\Phi_1(R_1\Phi_1 - d\Phi_2)}{4k_c d^2}(\sin\alpha, \cos\alpha) \tag{36}$$

Note that, in these formulas, it is possible to specify a different degree of expansion in λ if required to account for second- or higher-order terms. In Eq. (36), the gravity gradient torque in Eq. (15) is excluded, assuming that, for GEO, this torque is significantly less than the electrostatic torque in Eq. (14).

Substituting Eqs. (35) and (36) into Eqs. (13), (32), and (33), the simplified nonlinear equations are written as

$$J(\ddot{\theta} - \ddot{\alpha}) = \lambda^3 \frac{3R_1}{2k_c d^2}\Phi_1\left(\frac{R_1}{3d}\Phi_1 + \Phi_2\right)\sin 2\theta \tag{37}$$

$$\ddot{\alpha} = 2\frac{n - \dot{\alpha}}{d}\dot{d} + \frac{3}{2}n^2\sin 2\alpha + \frac{1}{d}[(a_p + u_y)\sin\alpha - u_x\cos\alpha] \tag{38}$$

$$\ddot{d} = d(3n^2\sin^2\alpha - 2n\dot{\alpha} + \dot{\alpha}^2) - (u_y + a_p)\cos\alpha - u_x\sin\alpha + \lambda\frac{7R_1\Phi_1(R_1\Phi_1 - d\Phi_2)}{4k_c m_* d^2} \tag{39}$$

Equations (38) and (39) are independent of the pitch attitude angle θ and coincide with equation 18 in Ref. [26]; therefore, in this case, the control laws using Eqs. (21) and (22) can be used from Ref. [26]:

$$u_x = c_\alpha \sin\alpha + c_{\dot{\alpha}}\dot{\alpha} \tag{40}$$

$$u_y = c_{\dot{d}}\dot{d} \tag{41}$$

The next step is to choose the attitude control law to stabilize the equation of motion in Eq. (37).

IV. Stability of Charged Closed-Loop Attitude Motion

It is possible to control the attitude motion using only the magnitude and sign of the electrical charge of the tug. This concept is explored in the following developments for a range of feedback control formulations. The general control law of the electrical change is given as

$$\Phi_1 = \bar{\Phi}_1(1 + \kappa\dot{\theta}f(\theta)) \quad (\bar{\Phi}_1 < 0) \tag{42}$$

where $f(\theta)$ is the periodic function, and κ is a constant feedback control parameter. Thus, this control provides the nominal repulsing potential $\bar{\Phi}_1$ if the debris is not tumbling, and it adds rate proportional feedback if the debris is tumbling. However, as discussed for the puller configuration with debris detumbling in Ref. [27], the rate damping is only possible for particular relative orientation angles θ. Prior work only considered $\sin(2\theta)$-type rate feedback modulations [8,27]. In this Note, two types of the function $f(\theta)$ are considered:

$$f(\theta) = \sin(i\theta), \quad \text{odd function with} \quad i = 1, 2, \ldots,$$
$$f(\theta) = \cos(i\theta), \quad \text{even function with} \quad i = 0, 1, 2, \ldots$$

to explore more general control solution formulations.

A. Feedback Control with an Odd Control Function

The first type of the odd function $f(\theta)$ is represented as

$$f(\theta) = \sin(i\theta) \quad \text{with} \quad i = 1, 2, \ldots \tag{43}$$

Then, the first-order approximation of the electrostatic torque in Eq. (14) is written as

$$L_E(\theta, \dot{\theta}, d) = \Lambda_1\sin(2\theta) + \Lambda_2\dot{\theta}\sin(2\theta)\sin(i\theta) \tag{44}$$

$$\Lambda_1 = \lambda^3\frac{3\bar{\Phi}_1 R_1}{2k_c d^2}\left(\Phi_2 + \frac{R_1}{3d}\bar{\Phi}_1\right), \quad \Lambda_2 = \kappa\lambda^3\frac{3\bar{\Phi}_1 R_1}{2k_c d^2}\left(\Phi_2 + \frac{2R_1}{3d}\bar{\Phi}_1\right) \tag{45}$$

Let us assume that the control laws in Eqs. (40) and (41) provide the realization of a stable position of the equilibrium equations [Eqs. (38) and (39)]:

$$\alpha = 0, \qquad d = d_s \tag{46}$$

Equation (37) is thus rewritten as

$$\ddot{\theta} + \Omega^2\sin(2\theta) = \xi\dot{\theta}\sin(2\theta)\sin(i\theta) \tag{47}$$

with the following simulation parameter definitions:

$$\Omega^2 = -\frac{\Lambda_1(d = d_s)}{J} = -\lambda^3\frac{3\bar{\Phi}_1 R_1}{2Jk_c d_s^2}\left(\Phi_2 + \frac{R_1}{3d_s}\bar{\Phi}_1\right) \tag{48}$$

$$\xi = \frac{\Lambda_2(d = d_s)}{J} = \kappa\lambda^3\frac{3\bar{\Phi}_1 R_1}{2Jk_c d_s^2}\left(\Phi_2 + \frac{2R_1}{3d_s}\bar{\Phi}_1\right) \tag{49}$$

The debris shape to separation distance constraint in Eq. (34) is rewritten into the following inequality expression:

$$\frac{R_1}{3d} \ll 1 \tag{50}$$

Next, the standard assumption is made that

$$\Omega^2 > 0 \tag{51}$$

As can be seen from Eq. (44), this torque becomes zero at the points

$$\theta = \pm k\frac{\pi}{2}, \qquad (k = 0, 1, 2, \ldots) \tag{52}$$

Using the linearized rotational equation in Eq. (47), the points

$$\theta_s = 0 \pm k\pi \tag{53}$$

correspond to the stable equilibrium position, and the points

$$\theta_u = \frac{\pi}{2} \pm k\pi \tag{54}$$

correspond to the unstable equilibrium position.

In a small neighborhood of the stable equilibrium position,

$$\theta_s = 0 \tag{55}$$

which allows Eq. (47) to be reduced to

$$\ddot{\theta} + 2\Omega^2\theta = 2n\xi\dot{\theta}\theta^2 \tag{56}$$

Next, Eq. (56) is rewritten through the use of a dimensionless time $\tau = \sqrt{2}\Omega t$ to a very simple form:

$$\ddot{\theta} + \theta = \varepsilon\theta'\theta^2 \tag{57}$$

Here, the differentiation notation

$$()' = \frac{\mathrm{d}}{\mathrm{d}\tau}()$$

is used and the following dimensionless small parameter ε is introduced:

$$\varepsilon=\frac{\sqrt{2}n\xi}{\Omega}=-\kappa\frac{\lambda n}{d_s}\sqrt{-\frac{2\lambda R_1\Phi_{10}(3d_s\Phi_2+R_1\Phi_{10})}{Jd_sk_c}}\cdot\frac{3d_s\Phi_2+2R_1\Phi_{10}}{3d_s\Phi_2+R_1\Phi_{10}} \tag{58}$$

For $\varepsilon=0$, Eq. (57) corresponds to an equation of unperturbed motion:

$$\theta''+\theta=0 \tag{59}$$

and an energy integral

$$E=\frac{\theta'^2}{2}+\frac{\theta^2}{2} \tag{60}$$

Using the following initial conditions,

$$\tau=0:\quad \theta=\theta_m,\quad \dot{\theta}=0 \tag{61}$$

this leads to the initial energy expression of the form

$$E=\frac{\theta_m^2}{2} \tag{62}$$

As a result, Eq. (59) has the following general solution:

$$\theta=\theta_m\cos t \tag{63}$$

From Eq. (62) follows an elegantly simple formula for the pitch attitude angle oscillation amplitude:

$$\theta_m=\pm\sqrt{2E} \tag{64}$$

The differentiation of Eq. (60) by Eq. (56) yields

$$\frac{\mathrm{d}E}{\mathrm{d}\tau}=(\theta''+\theta)\theta'=\varepsilon(\theta'\theta)^2 \tag{65}$$

and

$$\frac{\mathrm{d}|\theta_m|}{\mathrm{d}\tau}=\varepsilon\frac{(\theta'\theta)^2}{\theta_m} \tag{66}$$

The amplitude $|\theta_m|$ in the closed neighborhood of the equilibrium in Eq. (55) decreases with time if $\varepsilon<0$. This is satisfied according to Eq. (58) only when the coefficient

$$\kappa>0 \tag{67}$$

Thus, the formula in Eq. (66) shows that the control law in Eq. (42) leads to a decrease in the amplitude of small oscillations of the debris in the small neighborhood of a stable equilibrium position in Eq. (55). On the other hand, it is easy to see that the factor in Eq. (66)

$$\left[\frac{(\theta'\theta)^2}{\theta_m}\right] \tag{68}$$

for the small vicinity of a stable equilibrium position in Eq. (55) has the third order of smallness. In other words, the oscillations amplitude of the pitch attitude angle in the vicinity of the point in Eq. (55) will decrease very slowly.

B. Feedback Control with an Even Control Function

Next, an even function $f(\theta)$ is considered to be of the form

$$f(\theta)=\cos(i\theta)\quad\text{with}\quad i=0,1,2,\ldots \tag{69}$$

Here, the first-order approximation of the electrostatic torque in Eq. (14) is written as

$$L_E(\dot{\theta},d)=\Lambda_1\sin(2\theta)+\Lambda_2\dot{\theta}\sin(2\theta)\cos(i\theta) \tag{70}$$

Performing transformations similar to those made previously in Eqs. (47–57) provides the small neighborhood of the equilibrium position the equation of the attitude motion in the dimensionless form:

$$\theta''+\theta=\varepsilon\theta'\theta \tag{71}$$

For $\varepsilon=0$, this equation corresponds to the equation of unperturbed motion in Eq. (59):

$$\theta''+\theta=0 \tag{72}$$

The derivative of the energy integral in Eq. (60), taking into account Eq. (71), yields

$$\frac{\mathrm{d}E}{\mathrm{d}\tau}=(\theta''+\theta)\theta'=\varepsilon\theta'^2\theta \tag{73}$$

The averaging of Eq. (73) over the period of the unperturbed solution in Eq. (63) leads to the equation

$$\bar{E}_\tau=\left(\overline{\frac{\mathrm{d}E}{\mathrm{d}\tau}}\right)=\frac{\varepsilon}{2\pi}\int_0^{2\pi}\theta'^2\theta\,\mathrm{d}\tau=\frac{\varepsilon\theta_m^3}{2\pi}\int_0^{2\pi}\sin^2\tau\cos\tau\,\mathrm{d}\tau=0 \tag{74}$$

Hence, it is clear that the average energy does not change with time; therefore, according to Eq. (63), the average oscillations amplitude remains constant:

$$|\bar{\theta}_m|=\text{const} \tag{75}$$

and detumbling control algorithms with the even function in Eq. (69) do not yield a stabilizing result.

C. Numerical Simulation of the Odd Control Solution

For numerical simulations, system parameters are chosen as in Table 1. The stabilizing control law in Eq. (43) is considered for $i=2$ to relate to prior work in Ref. [27] that also used $\sin(2\theta)$ to stabilize the debris attitude in a puller configuration:

$$\Phi_1=\bar{\Phi}_1(1+\kappa\dot{\theta}\sin 2\theta)\quad(\bar{\Phi}_1<0) \tag{76}$$

The differential equation in Eq. (56) is integrated with the following initial conditions:

$$\theta_0=0.5,\qquad \dot{\theta}_0=0$$

Figures 2 and 3 show the time history (in hours) of the pitch attitude angle θ (in radians) and the oscillations amplitude $\pm\theta_m$ (in radians) for different values of $\kappa=10$ and $\kappa=100$. Figures 4 and 5 show the corresponding tug electrostatic control potentials. These control

Table 1 Simulation parameters for the detumble control scenario

Parameter	Value
j, km^2	50
$\Phi_2=\lvert\Phi_1\rvert$, kV	20
R_1, m	0.5
$R_{2,a}=R_{2,b}$, m	0.5909
$R_{2,c}$, m	0.5909
l, m	0.5
i	2
d_s, m	1.997

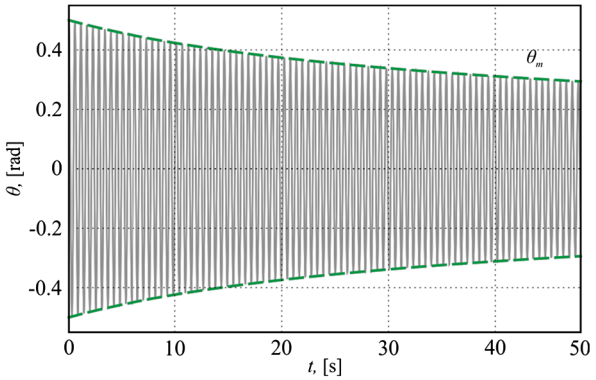

Fig. 2 Time history of the pitch attitude angle θ (solid) and θ_m, $-\theta_m$ (dotted) for Eq. (57) ($\kappa = 10$).

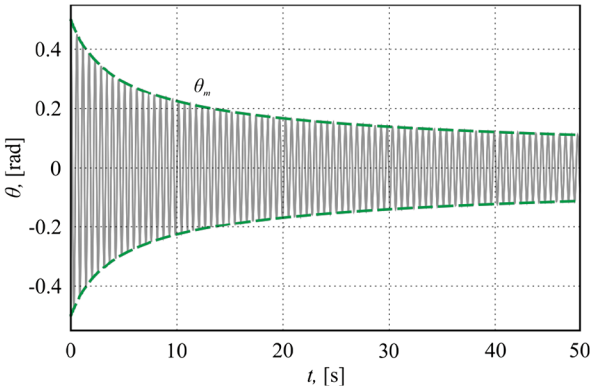

Fig. 3 Time history of the pitch attitude angle θ (solid) and θ_m, $-\theta_m$ (dotted) for Eq. (57) ($\kappa = 100$).

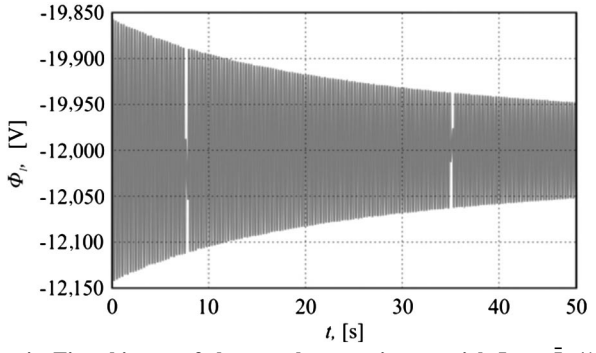

Fig. 4 Time history of the tug electrostatic potential $\Phi_1 = \bar{\Phi}_1(1 + \kappa\dot{\theta}\sin 2\theta)$ for $\kappa = 10$.

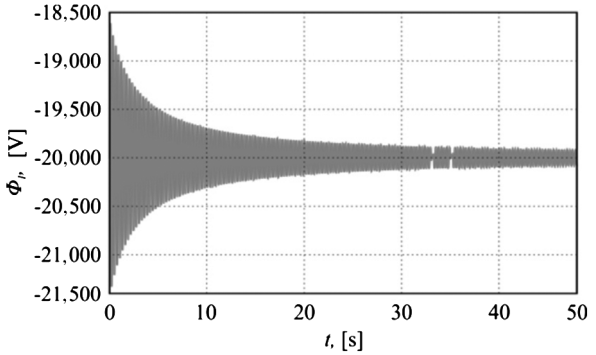

Fig. 5 Time history of the tug electrostatic potential $\Phi_1 = \bar{\Phi}_1(1 + \kappa\dot{\theta}\sin 2\theta)$ for $\kappa = 100$.

potentials are still practical to implement because they are similar in magnitude to naturally occurring potentials for GEO objects during emergence from the Earth's shadow.

V. Numerical Simulation

This section shows with numerical simulations how the parameters of the proposed feedback control affect the stability of the system. In all cases, the control goal is to reduce the debris tumble rate (i.e., $\dot{\theta} \to 0$) and keep the spacecraft aligned in a leader–follower configuration (i.e., $\alpha = \dot{\alpha} = 0$). The investigation is performed by numerical integration of the initial equations of motion in Eqs. (13), (32), and (33) for the control laws [Eqs. (40), (41), and (76)]:

$$u_x = c_\alpha \sin\alpha + c_{\dot{\alpha}}\dot{\alpha} \tag{77}$$

$$u_y = c_{\dot{d}}\dot{d} \tag{78}$$

$$\Phi_1 = \bar{\Phi}_1(1 + \kappa\dot{\theta}\sin 2\theta)(\bar{\Phi}_1 < 0) \tag{79}$$

The differential equations [Eqs. (13), (32), and (33)] are integrated with the following initial conditions:

$$\theta_0 = 0.5\ \text{rad}, \quad \dot{\theta}_0 = -0.10\ \text{rad/s}$$
$$\alpha_0 = 0.5, \quad \dot{\alpha}_0 = 0 \tag{80}$$

$$d_0 = 2\ \text{m}, \qquad \dot{d}_0 = 0 \tag{81}$$

The gravitational torque in Eq. (15) for the GEO is neglected in Eq. (13); it is considered small as compared with the electrostatic torque in Eq. (14). Additional simulation parameters of the system are given in Table 2.

Figures 6–13 depict the time dependence of the pitch attitude angle θ, the angle between the local-horizontal line of the tug and the line connecting the tug and debris α, the distance between the space tug and the debris d, and the charge of the space tug Φ_1 for various tugs' thrust force P.

The simulation results for the tug's thrust force of $P = 5$ mN are shown in Figs. 6–9. Figures 7 and 8 illustrate that the separation distance and heading are stabilized and the average indicator is equal to $\lambda = l/d \approx 0.21$ for $t > 3$ h. Note that the simulation with a stronger thruster force P results in a smaller separation distance because the same nominal electrostatic repulsor potential is used in both cases. Thus, the higher thrust results in the debris–tug separation being more compressed. Similar stability properties are also observed for a larger tug thrust force value of $P = 20$ mN (Figs. 10–13) and $\lambda \approx 0.36$ (Fig. 12). Regarding the ability to detumble the debris object while in a pusher configuration, the initial spin rate is first quickly reduced, but then the convergence rate slows down as predicted with the aforementioned linearized analysis. One reason the debris rate damping control is at first more effective is that the separate distance is initially not constant but oscillating about a nominal value. This causes the debris and tug to be periodically closer than the nominal distance, and thus the electrostatic forces and torques are larger with the shorter separation distance. As the separation distance settles to a steady value, the debris rate damping continues but with less effectiveness because the electrostatic forces and torques are now reduced in comparison to the initial transient performance. Another reason for the slowing convergence rate is analytically predicted in Sec. IV.A, in which the convergence is shown to slow down as the desired state is approached. The period in which the relative motion is

Table 2 Numerical simulation parameters

Parameter	Value
m_1, kg	300
m_2, kg	1000
κ	100
c_α	−0.0001
$c_{\dot{\alpha}}$	−0.001
$c_{\dot{d}}$	−0.001
P, mN	5; 20

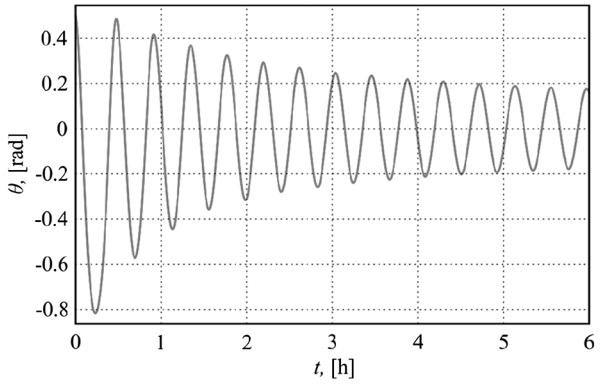

Fig. 6 Time history of the pitch attitude angle θ for the tug's thrust force of $P = 5$ mN.

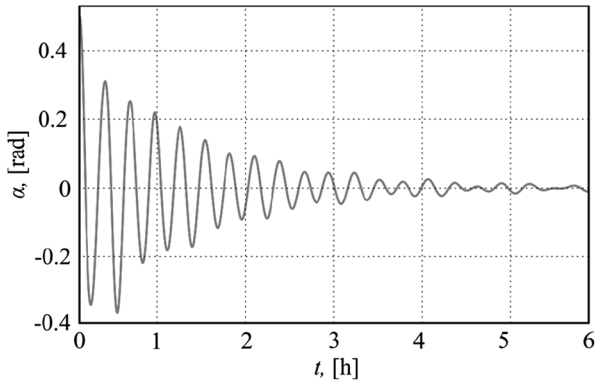

Fig. 7 Time history of the angle α for the tug's thrust force of $P = 5$ mN.

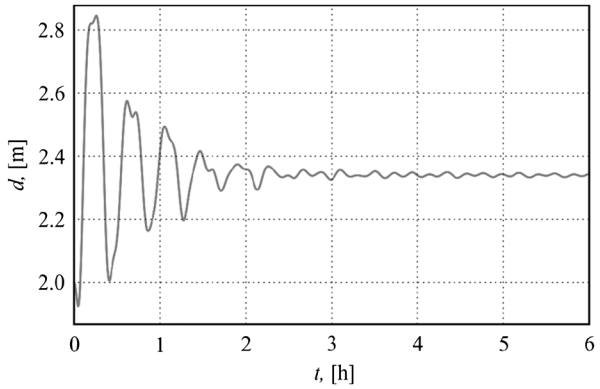

Fig. 8 Time history of the distance between the bodies d for the tug's thrust force of $P = 5$ mN.

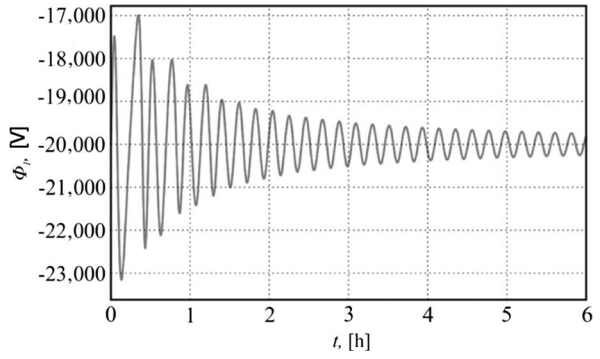

Fig. 9 Time history of the electrical charge of the tug $\Phi_1 = \bar{\Phi}_1(1 + \kappa\dot{\theta}\sin 2\theta)$ for the tug's thrust force of $P = 5$mN.

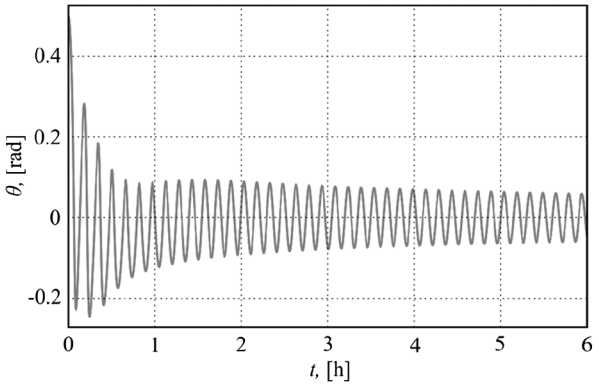

Fig. 10 Time history of the pitch attitude angle θ for the tug's thrust force of $P = 20$ mN.

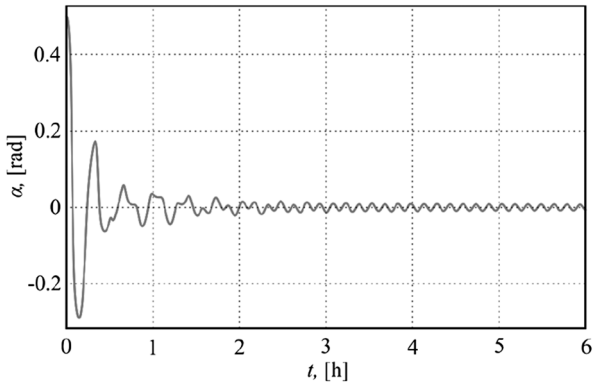

Fig. 11 Time history of the angle α for the tug's thrust force of $P = 20$ mN.

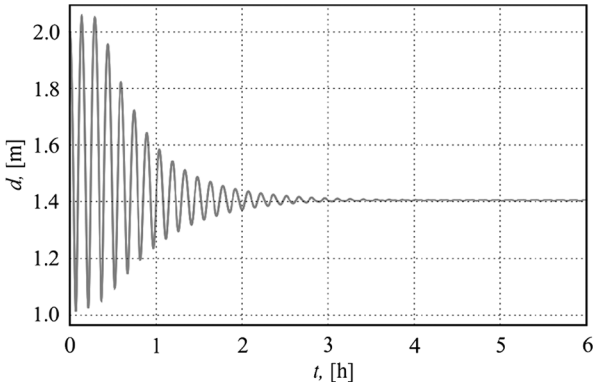

Fig. 12 Time history of the distance between the bodies d for the tug's thrust force of $P = 20$ mN.

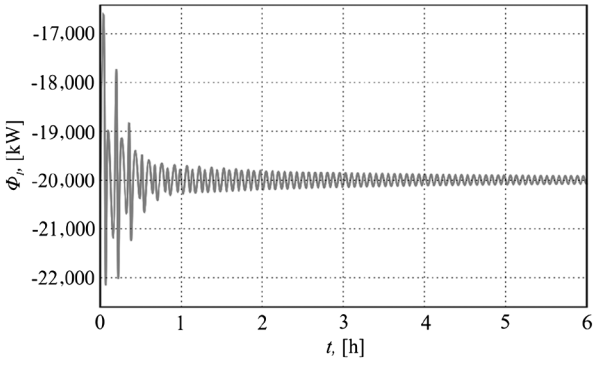

Fig. 13 Time history of the electrical charge of the tug $\Phi_1 = \bar{\Phi}_1(1 + \kappa\dot{\theta}\sin 2\theta)$ for the tug's thrust force of $P = 20$ mN.

still settling to the steady-state location yields a stronger detumble performance, illustrating a direction of future research to investigate this coupled behavior further.

VI. Conclusions

This study explores the relative motion and debris spin rate stability of a pusher electrostatic tug configuration. A simplified electrostatic force and torque formulation is employed to perform an analytical stability analysis for small departure motions. Two detumble control formulations are investigated with odd and even feedback functions. Although the odd formulation does yield a stabilizing tumble response that brings the tumble rate to zero, the even formulation is shown to not change the tumble error energy. In this analytical analysis, the nominal separation location is held fixed in an alongtrack configuration. A challenge with the detumble convergence rate from this control structure is analytically discussed. The numerical simulations illustrate the predicted relative motion and tumble rate stability for a range of tug force configurations, illustrating the robustness to such control parameter variations.

Appendix: Charged Model Parameter Definitions

The following parameter definitions allow for the compact formulation in Eq. (23):

$$
\begin{aligned}
a_{E,x}(\theta,d) &= \Phi_1 dlR_1(2l-R_2)G_-G_+[2l^2+R_2(l-4R_{2,c})]\\
&\quad+\Phi_2 lR_1(2l-R_2)[lG_-G_+(-2l+3R_2)R_{2,c}\\
&\quad+2dlG_-R_2(-l+R_{2,c})+2dlG_+R_2(-l+R_{2,c})]
\end{aligned}
$$

$$
\begin{aligned}
b_{E,x}(\theta,d) &= \Phi_1 2dl(G_--G_+)R_2[dR_1G_-^3G_+(2l-R_2)R_{2,c}\\
&\quad+dR_1G_-^2G_+^2(2l-R_2)R_{2,c}+dR_1G_-G_+^3(2l-R_2)R_{2,c}\\
&\quad+d^2R_1(lG_-^2G_+(-2l+R_2)+lG_-G_+^2(-2l+R_2)\\
&\quad-2(G_-^3+G_+^3)(l^2-R_2R_{2,c}))]\\
&\quad+\Phi_2 2dl(G_--G_+)R_2[d^2(G_-^3G_+(2l-R_2)+G_-G_+^3(2l-R_2)\\
&\quad+2lR_1G_+^2R_2+G_-^2(G_+^2(2l-R_2)+2lR_1R_2))(l-R_{2,c})\\
&\quad+dlR_1G_-^2G_+(2l-R_2)R_{2,c}-lR_1G_-^3G_+(2l-R_2)R_{2,c}\\
&\quad+dlR_1G_-G_+^2(2l-R_2)R_{2,c}-lR_1G_-^2G_+^2(2l-R_2)R_{2,c}\\
&\quad-lR_1G_-G_+^3(2l-R_2)R_{2,c}-2dlR_1G_-^3(-l+R_2)R_{2,c}\\
&\quad-2dlR_1G_+^3(-l+R_2)R_{2,c}]
\end{aligned}
$$

$$
\begin{aligned}
c_{E,x}(\theta,d) &= \Phi_1[2d^4G_-^3G_+R_1R_2^2(l-2R_{2,c})\\
&\quad+2d^4G_-G_+^3R_1R_2^2(l-2R_{2,c})+2d^3G_-^4G_+R_1(2l-R_2)R_2R_{2,c}\\
&\quad+2dG_-^4G_+^3R_1(2l-R_2)R_2R_{2,c}+2d^3G_-G_+^4R_1(2l-R_2)R_2R_{2,c}\\
&\quad+2dG_-^3G_+^4R_1(2l-R_2)R_2R_{2,c}+G_-^4G_+^4R_1(2l-R_2)(2l+R_2)R_{2,c}\\
&\quad-4d^4G_-^4R_1R_2(l^2-R_2R_{2,c})+4d^4G_+^4R_1R_2(-l^2+R_2R_{2,c})]\\
&\quad+\Phi_2[2d^4G_-^4G_+(2l-R_2)R_2(l-R_{2,c})\\
&\quad+2d^4G_-G_+^4(2l-R_2)R_2(l-R_{2,c})+4d^4lG_-^3R_1R_2^2(l-R_{2,c})\\
&\quad+4d^4lG_+^3R_1R_2^2(l-R_{2,c})+4d^3lG_-^4R_1(l-R_2)R_2R_{2,c}\\
&\quad+4d^3lG_+^4R_1(l-R_2)R_2R_{2,c}+2lG_-^4G_+^3R_1(2l-R_2)R_2R_{2,c}\\
&\quad+2lG_-^3G_+^4R_1(2l-R_2)R_2R_{2,c}\\
&\quad-2d^2lG_-G_+(G_-^3+G_+^3)R_1(2l-R_2)R_2R_{2,c}\\
&\quad+2d^3lG_-^3G_+R_1R_2^2R_{2,c}+2d^3lG_-G_+^3R_1R_2^2R_{2,c}\\
&\quad-4dlG_-^3G_+^3R_1R_2^2R_{2,c}+4dlG_-^4G_+^2R_1R_2(-l+R_2)R_{2,c}\\
&\quad+4dlG_-^2G_+^4R_1R_2(-l+R_2)R_{2,c}-dG_-^4G_+^4(2l-R_2)(-2l+3R_2)R_{2,c}\\
&\quad+4d^4lG_-^2G_+R_1R_2^2(-l+R_{2,c})+4d^4lG_-G_+^2R_1R_2^2(-l+R_{2,c})]
\end{aligned}
$$

$$
\begin{aligned}
a_{E,y}(\theta,d) &= -\Phi_1 dlR_1(2l-R_2)G_-G_+[2l^2+R_2(l-4R_{2,c})]\\
&\quad+\Phi_2 lR_1(2l-R_2)[-lG_-G_+(-2l+3R_2)R_{2,c}\\
&\quad+2dlG_+R_2(l-R_{2,c})-2dlG_-R_2(-l+R_{2,c})]
\end{aligned}
$$

$$
\begin{aligned}
b_{E,y} &= \Phi_1 2dl(G_--G_+)R_2[dG_-^3G_+R_1(2l-R_2)R_{2,c}\\
&\quad+dG_-^2G_+^2R_1(2l-R_2)R_{2,c}+dG_-G_+^3R_1(2l-R_2)R_{2,c}\\
&\quad+d^2R_1(lG_-^2G_+(-2l+R_2)+lG_-G_+^2(-2l+R_2)\\
&\quad-2(G_-^3+G_+^3)(l^2-R_2R_{2,c}))]\\
&\quad+\Phi_2 2dl(G_--G_+)R_2[d^2(G_-^3G_+(2l-R_2)\\
&\quad+G_-G_+^3(2l-R_2)+2lG_+^2R_1R_2+G_-^2(G_+^2(2l-R_2)\\
&\quad+2lR_1R_2))(l-R_{2,c})+dlG_-^2G_+R_1(2l-R_2)R_{2,c}\\
&\quad-lG_-^3G_+R_1(2l-R_2)R_{2,c}+dlG_-G_+^2R_1(2l-R_2)R_{2,c}\\
&\quad-lG_-^2G_+^2R_1(2l-R_2)R_{2,c}-lG_-G_+^3R_1(2l-R_2)R_{2,c}\\
&\quad-2dlG_-^3R_1(-l+R_2)R_{2,c}-2dlG_+^3R_1(-l+R_2)R_{2,c}]
\end{aligned}
$$

Acknowledgment

This study was supported by the Russian Foundation for Basic Research (RFBR 18-01-00215-A).

References

[1] Liou, J.-C., Johnson, N., and Hill, N., "Controlling the Growth of Future LEO Debris Populations with Active Debris Removal," *Acta Astronautica*, Vol. 66, Nos. 5–6, 2010, pp. 648–653. doi:10.1016/j.actaastro.2009.08.005

[2] Oltrogge, D. L., Alfano, S., Law, C., Cacioni, A., and Kelso, T. S., "A Comprehensive Assessment of Collision Likelihood in Geosynchronous Earth Orbit," *Acta Astronautica*, Vol. 147, June 2018, pp. 316–345. doi:10.1016/j.actaastro.2018.03.017

[3] Anderson, P. V., and Schaub, H., "Local Debris Congestion in the Geosynchronous Environment with Population Augmentation," *Acta Astronautica*, Vol. 94, No. 2, Feb. 2014, pp. 619–628. doi:10.1016/j.actaastro.2013.08.023

[4] Binz, C. R., Davis, M. A., Kelm, B. E., and Moore, C. I., "Optical Survey of the Tumble Rates of Retired GEO Satellites," *Advanced Maui Optical and Space Surveillance Technologies Conference*, Vol. 1, 2014, p. 61.

[5] Bombardelli, C., and Pelaez, J., "Ion Beam Shepherd for Contactless Space Debris Removal," *Journal of Guidance, Control, and Dynamics*, Vol. 34, No. 3, May–June 2011, pp. 916–920. doi:10.2514/1.51832

[6] Kumar, R., and Sedwick, R. J., "Despinning Orbital Debris Before Docking Using Laser Ablation," *Journal of Spacecraft and Rockets*, Vol. 52, No. 4, 2015, pp. 1129–1134. doi:10.2514/1.A33183

[7] Schaub, H., and Moorer, D. F., "Geosynchronous Large Debris Reorbiter: Challenges and Prospects," *Journal of the Astronautical Sciences*, Vol. 59, Nos. 1–2, 2014, pp. 161–176. doi:–10.1007/s40295-013-0011–8

[8] Stevenson, D., "Remote Spacecraft Attitude Control by Coulomb Charging," Ph.D. Dissertation, Aerospace Engineering Sciences Dept., Univ. of Colorado, Boulder, CO, May 2015.

[9] Shibata, T., Bennett, T., and Schaub, H., "Prospects of a Hybrid Magnetic/Electrostatic Sample Container Retriever," *9th International Workshop on Satellite Constellations and Formation Flying*, Paper IWSCFF 17-15, Boulder, CO, June 2017.

[10] Hogan, E., and Schaub, H., "Relative Motion Control for Two-Spacecraft Electrostatic Orbit Corrections," *Journal of Guidance, Control, and Dynamics*, Vol. 36, No. 1, Jan.–Feb. 2013, pp. 240–249. doi:10.2514/1.56118

[11] Bennett, T., and Schaub, H., "Touchless Electrostatic Detumble Of A Representative Box-And-Panel Spacecraft Configuration," *European Conference on Space Debris*, ESOC, Darmstadt, Germany, April 2017.

[12] Mullen, E. G., Gussenhoven, M. S., Hardy, D. A., Aggson, T. A., and Ledley, B. G., "SCATHA Survey of High-Voltage Spacecraft Charging in Sunlight," *Journal of Geophysical Research*, Vol. 91, No. A2, 1986,

pp. 1474–1490.
doi:10.1029/JA091iA02p01474
[13] Fennell, J. F., and Roeder, J. L., "HEO Satellite Surface and Frame Charging and SCATHA Low-Level Frame Charging," The Aerospace Corporation TR-2007(8570)-1, El Segundo, CA, Nov. 2007.
[14] Fennell, J. F., Koons, H. C., Leung, M. S., and Mizera, P. F., "A Review of SCATHA Satellite Results: Charging and Discharging," Space Division Air Force Systems Command, Los Angeles Air Force Station TR SD-TR-85-27, Los Angeles, CA, Aug. 1985.
[15] Olsen, R. C., and Whipple, E. C., "Analysis of Differential and Active Charging Phenomena on ATS-5 and ATS-6," NASA TR NASA-CP-163433, 1980.
[16] Whipple, E. C., and Olsen, R. C., "Importance of Differential Charging for Controlling Both Natural, and Induced Vehicle Potentials on ATS-5, and ATS-6," *Proceedings of the 3rd Spacecraft Charging Technology Conference*, NASA CP 2182, Nov. 1980, pp. 887–893.
[17] Stevenson, D., and Schaub, H., "Multi-Sphere Method for Modeling Electrostatic Forces and Torques," *Advances in Space Research*, Vol. 51, No. 1, Jan. 2013, pp. 10–20.
doi:10.1016/j.asr.2012.08.014
[18] Stevenson, D., and Schaub, H., "Optimization of Sphere Population for Electrostatic Multi Sphere Model," *IEEE Transactions on Plasma Science*, Vol. 41, No. 12, Dec. 2013, pp. 3526–3535.
doi:10.1109/TPS.2013.2283716
[19] Chow, P., Hughes, J., Bennett, T., and Schaub, H., "Automated Sphere Geometry Optimization for the Volume Multi-Sphere Method," *AAS/AIAA Spaceflight Mechanics Meeting*, AAS Paper 16-472, Napa Valley, CA, Feb. 2016, pp. 2223–2240.
[20] Ingram, G., Hughes, J., Bennett, T., Reilly, C., and Schaub, H., "Autonomous Volume Multi-Sphere-Model Development Using Electric Field Matching," *AAS Spaceflight Mechanics Meeting*, AAS Paper 17-451, San Antonio, TX, Feb. 2017.
[21] Smythe, W. R., *Static and Dynamic Electricity*, 3rd ed., McGraw–Hill, 1968, Chap. 2.
[22] Zhang, F., *The Schur Complement and Its Applications*, Springer, Boston, MA, 2005, Chap. 1.
[23] Wolfram, S., *The Mathematica Book*, 5th ed., Cambridge Univ. Press, Cambridge, England, U.K., 2003.
[24] Alfriend, K. T., Vadali, S. R., Gurfil, P., How, J. P., and Breger, L. S., "Linear Equations of Relative Motion," *Spacecraft Formation Flying*, Butterworth-Heinemann, Oxford, England, U.K., 2010, pp. 83–121.
doi:10.1016/B978-0-7506-8533-7.00210-4
[25] Hogan, E. A., and Schaub, H., "Attitude Parameter Inspired Relative Motion Descriptions for Relative Orbital Motion Control," *Journal of Guidance, Control, and Dynamics*, Vol. 37, No. 3, 2014, pp. 741–749.
doi:10.2514/1.60626
[26] Aslanov, V. S., and Yudintsev, V. V., "Motion Control of Space Tug During Debris Removal by a Coulomb Force," *Journal of Guidance, Control, and Dynamics*, Vol. 41, No. 7, March 2018, pp. 1476–1484.
doi:10.2514/1.G003251
[27] Schaub, H., and Stevenson, D., "Prospects of Relative Attitude Control Using Coulomb Actuation," *Journal of Astronautical Sciences*, Vol. 60, No. 3, 2013, pp. 258–277.
doi:10.1007/s40295-015-0048-y